The GCM Oriented Calipso Cloud Product (CALIPSO-GOCCP)

H. Chepfer[1], S. Bony[1], D. Winker[2], G. Cesana[3], JL. Dufresne[1], P. Minnis[2], C. J. Stubenrauch[3], S. Zeng[4]

[1] LMD/IPSL, Univ. Paris 06, CNRS, Paris, France.

[2] NASA/LaRC, Hampton, VA, USA.

[3] LMD/IPSL, CNRS, Ecole Polytechnique, Palaiseau, France.

[4] LOA, Univ. Lille, Lille, France

1.Introduction

2. Processing of Calipso level 1 data

     2.a. Calculation of the scattering Ratio

     2.b. Definition of cloud diagnostics

     2.c. June-July-August and January-February-March results

3. Sensitivity to the horizontal and vertical averaging, and to cloud detection thresholds

     3.a. Sensitivity to horizontal sampling

     3.b. Sensitivity to the vertical resolution

     3.c. Sensitivity to the cloud detection threshold

4. Day-night and regional cloud variations

     4.a. Day-Night differences

     4.b. A regional scale example: along the GPCI transect

5. Comparison with other cloud climatologies

6. Conclusion

Abstract. This paper presents the GCM-Oriented Cloud-Aerosol Lidar and Infrared Pathfinder Satellite Observations (CALIPSO) Cloud Product (CALIPSO-GOCCP) designed to evaluate the cloudiness simulated by General Circulation Models (GCMs). For this purpose, CALIOP L1 data are processed following the same steps as in a lidar simulator used to diagnose the model cloud cover that CALIPSO would observe from space if the satellite was flying above an atmosphere similar to that predicted by the GCM. Instantaneous profiles of the lidar Scattering Ratio (SR) are first computed at the highest horizontal resolution of the data but at the vertical resolution typical of current GCMs, and then cloud diagnostics are inferred from these profiles: vertical distribution of cloud fraction, horizontal distribution of low-mid-high and total cloud fractions, instantaneous SR profiles, and SR histograms as a function of height. Results are presented for different seasons (January-February-March 2007-2008 and June-July-August 2006-2007-2008), and their sensitivity to parameters of the lidar simulator is investigated. It is shown that the choice of the vertical resolution and of the SR threshold value used for cloud detection can modify the cloud fraction by up to 0.20, particularly in the shallow cumulus regions. The tropical marine low-level cloud fraction is larger during nighttime (by up to 0.15) than during day-time. The histograms of SR characterize the cloud types encountered in different regions.

The GOCCP high-level cloud amount is similar to that from TOVS and AIRS. The low-level and mid-level cloud fractions are larger than those derived from passive remote sensing (ISCCP, MODIS-CERES POLDER, TOVS Path B, AIRS-LMD), because the latter ones only provide information on the uppermost cloud layer.

Introduction

The definition of clouds or cloud types is not unique. It differs among observations (e.g. clouds detected by a lidar may not be detected by a radar or by passive remote sensing), and between models and observations (e.g. models predict clouds at each atmospheric level where condensation occurs, while observations may not detect clouds overlapped by thick upper-level clouds). A comparison between modelled and observed clouds thus requires a consistent definition of clouds, taking into account the effects of viewing geometry, sensors' sensitivity and vertical overlap of cloud layers. For this purpose, clouds simulated by climate models are often compared to observations through a model-to-satellite approach: model outputs are used to diagnose some quantities that would be observed from space if satellites were flying above an atmosphere similar to that predicted by the model [e.g., Yu et al., 1996, Stubenrauch et al. 1997, Klein and Jacob, 1999, Webb et al., 2001, Zhang et al., 2005, Bodas-Salcedo et al., 2008, Chepfer et al,. 2008, Marchand et al., 2009].

Within the framework of the Cloud Feedback Model Intercomparison Program (CFMIP, http://www.cfmip.net), a package named COSP ("CFMIP Observation Simulator Package") has been developed to compare in a consistent way the cloud cover predicted by climate models with that derived from different satellite observations. This package includes in particular an ISCCP (International Satellite Cloud Climatology Project) simulator [Klein and Jacob, 1999, Webb et al., 2001], a CloudSat simulator [Haynes et al., 2007], and a Cloud-Aerosol Lidar and Infrared Pathfinder Satellite Observations (CALIPSO) simulator [Chepfer et al., 2008). Additionally, it includes a Subgrid Cloud Overlap Profile Sampler [Klein and Jacob, 1999] that divides each model grid box into an ensemble of sub-columns generated stochastically and, in which the cloud fraction is assigned to be 0 or 1 at every model level, with the constraint that the cloud condensate and cloud fraction averaged over all sub-

columns is consistent with the grid-averaged model diagnostics and the cloud overlap assumption.

The purpose of this paper is to present a dataset, named CALIPSO-GOCCP, that diagnoses cloud properties from CALIPSO observations exactly in the same way as in the simulator (similar spatial resolution, same criteria used for cloud detection, same statistical cloud diagnostics). This ensures that discrepancies between model and observations reveal biases in the model's cloudiness rather than differences in the definition of clouds or of diagnostics.

Section 2 describes the processing of CALIPSO Cloud-Aerosol Lidar with Orthogonal Polarization (CALIOP) Level 1 data [Winker et al. 2007] leading to the GOCCP dataset, and presents globally-averaged results for June-July-August (JJA) 2006-2007-2008 and January-February-March (JFM) 2007-2008. The sensitivity of observed cloud diagnostics to the vertical resolution and to the cloud detection threshold is evaluated in Section 3. Day/night variabilities of cloud characteristics are discussed in Section 4, together with an illustration of GOCCP results along the Global Energy and Water Cycle Experiment (GEWEX) Pacific Cross-section Intercomparison transect (GPCI, http://gcss-dime.giss.nasa.gov/gpci/modsim_gpci_models.html). GOCCP results are then compared with other cloud climatologies in Section 5, and conclusions are drawn in Section 6.

2. Processing of CALIOP Level 1 data

2a. Calculation of the Scattering Ratio

Here we use the Attenuated Backscattered profile at 532nm (ATB, collection V2. 01) that is part of the CALIOP lidar Level 1 dataset. CALIOP is aboard CALIPSO, a nearly sun-synchronous platform that crosses the equator at about 0130 LST [Winker et al. 2007, 2009].

The original ATB horizontal resolution is 330 m below 8 km of altitude and 1 km above . The original ATB vertical resolution is 30 m below 8km of altitude and and 60 m above ; total of 583 vertical levels are distributed from the surface up to 40 km. The Molecular Density profile (MD) is derived from Goddard Modeling and Assimilation Office (GMAO) atmospheric profiles [Bey et al. 2001] for 33 vertical levels.

In the COSP software, both the CALIPSO and the CloudSat simulator results are computed on a vertical grid of 40 equidistant levels (height interval, Δz = 480 m) distributed from the sea level to 19 km. The ATB profile (583 vertical levels, Fig. 1a) and the MD profile (33 vertical levels) are each independently averaged or interpolated onto the 40-level vertical grid, leading to the ATB_{vert} and MD_{vert} profiles. This averaging significantly increases the ATB signal-to-noise ratio.

To convert the MD profile into molecular ATB, ATB_{vert} and MD_{vert} profiles are analyzed and averaged in cloud-free portions of the stratosphere: $22 < z < 25$ km for night time data ($20 < z < 25$ km for day time), and $28.5 < z < 35$km in the Southern Hemisphere ($60°s$ to $90°S$) during winter (June to October) to avoid Polar Stratospheric Clouds. At these altitudes z, ATB_{vert} and MD_{vert} profiles are each averaged horizontally over +/-33 profiles (+/-10 km) on both sides of a given profile.

The ratio between these two values ($R = <ATB_{vert}> / <MD_{vert}>$) in the cloud-free stratosphere is then used to scale the MD_{vert} profile into an ATtenuated Backscatter Molecular signal profile ($ATB_{vert,mol}$). This latter represents the ATB profile that would be measured in the absence of clouds and aerosols in the atmosphere. The lidar scattering ratio (SR) vertical profile is then computed by dividing the ATB_{vert} profile by the $ATB_{vert,mol}$ profile. Its horizontal resolution is 330 m and the vertical resolution (40 levels) is close to that of GCMs (Figures 1b,d and 2b,d)

Despite the vertical averaging, the signal-to-noise ratio remains low during daytime in clear-sky regions because of the large number of solar photons reaching the lidar's telescope

(Figures 2b and d). However, the laser light reflection on optically thick clouds decreases the signal-to-noise ratio in the stratosphere, giving anomalous R values. Therefore, daytime profiles with R values significantly different from those associated with nighttime profiles (R > 0.95 or R < 0.14) are rejected. They represent about 30% of the total number of Level 1 V2.01 daytime profiles (e.g., Figure 2c). Pixels located below and at the surface level are rejected by using the 'altitude-elevation' flag from level 1 CALIOP data.

2b. Definition of cloud diagnostics

Here we present how cloud detection is performed for each lidar profile, and then how monthly statistical summaries are produced.

(i) Cloud detection on a single profile

Several simple diagnostics are derived from the SR profile. Different SR thresholds are used to label each atmospheric layer (Figures 1d and 2d) as cloudy (SR > 5), clear (0.01 < SR < 1.2), fully attenuated (SR < 0.01), or unclassified (1.2 < SR < 5 or $ATB-ATB_{mol}$ < $2.5.10^{-3}$ $km^{-1}.sr^{-1}$) to avoid false cloud detection in the upper troposphere / lower stratosphere, where the ATB_{mol} is very low. We then determine if the profile contains at least one cloud layer within the low-level (P > 680 hPa), middle-level (440 < P < 680 hPa) and upper-level (P < 440 hPa) atmospheric layers, and in the whole column. To keep detailed information about the distribution of the lidar signal intensity, we also record the occurrence frequency of different SR values (we use 15 intervals of SR values, ranging from 0 to 100) as a function of height (y-axis) to built the histograms of SR values (referred to as SR CFAD532 in the GOCCP dataset).

(ii) Monthly cloud diagnostics

Monthly cloud fractions are then computed at each vertical level (or at low-, middle-, and upper-level layers) by dividing, for each longitude-latitude grid box (e.g. 1 deg x 1 deg or 2.5 deg x 2.5 deg), the number of cloudy profiles encountered during one month by the total number of instantaneous SR profiles (not fully attenuated) measured during that month. In the GOCCP database, cloud-layer diagnostics are referred to as " Low – Mid – Highlayered cloud fractions" and monthly mean three-dimensional distributions of the cloud fraction as "3D Cloud Faction".

Monthly SR histograms (which provide information about the variability of the SR signal) are also computed by accumulating the instantaneous SR histograms over a month in each grid box and each vertical layer. Each of these diagnostics has its counterpart included in the lidar simulator outputs of COSP.

2.c. June-July-August and January-February-March results

In this section we present the seasonal mean results for JJA and JFM obtained for the 40 levels vertical grid and for a horizontal resolution of 2.5° (latitude) x 3.75° (longitude).

    (i)   Maps of total and layered cloud fractions.

As shown by Table 1, the total cloud cover is larger over ocean (0.71) than over land (0.57), with a global average of 0.66. This is lower than the global cloud cover of 76% determined by Mace et al. [2009], using a combined CALIPSO-CloudSat product. The latter corresponds to the cloud cover of CALIOP-NASA L2, since CALIOP is sensitive to thinner clouds than CloudSat. For high clouds the horizontal averaging can be up to 80 km to detect subvisible cirrus, whereas CALIOP-GOCCP applies vertical averaging which is not sensitive to the detection of very thin cirrus. The analysis of Sassen and Wang [2008] using CloudSat data alone, leads to a cloud cover of 64.0% over ocean and of 54.7% over land, whereas CALIOP-

NASA L2 yields 84% and 63%, respectively. As expected, Figure 3a shows that the minimum total cloud cover occurs over sub-tropical deserts (Sahara, South Africa, Australia, etc), and the maxima are found over the Inter-Tropical Convergence Zone (ITCZ), in mid-latitudes storm tracks, and at the eastern sides of the ocean basins associated with persistent low-level stratiform cloudiness (Figure 3a). Maps of low-level, mid-level and upper-level cloud fractions (Figures 3b-h) show the predominance of low-level clouds over the oceans, both in the tropics and in the extra-tropics, and a striking land-sea constrast in the low-level cloud fraction. Low-level cloud fractions of about 0.3-0.4 are found in the trade wind areas (typically covered by shallow cumulus clouds), while amounts exceeding 0.6 occur in the mid-latitudes. Small low-level cloud fractions are reported only in the deep convective regions (warm pools, ITCZ), where thick upper-level clouds attenuate the lidar signal so much that low-level clouds cannot be detected.

At the global scale,, the change in total cloud amount is less than 0.01 between JJA and JFM (Table 1). This is in agreement with other observations: when considering the whole globe, cloud fraction does not change with season; only its distribution changes. ISCCP and TOVS Path-B report 0.65 / 0.70 in JJA and 0.67 / 0.72 in JFM, respectively. The main seasonal cloud fraction variation (Figures 3e-h for JJA vs. Figures 3a-d for JFM) occurs in tropical regions (between 30°N and 20°S), where both oceanic and land cloud cover changes follow the seasonal latitudinal migration of the ITCZ. The mid and high cloud cover seasonal variations are similar (Figure 3) because the mid-level clouds are often associated with high clouds. The largest seasonal variation for both cloud layers is associated with deep convection over continents.

    (ii)   Vertical distribution of clouds.

The zonally averaged vertical distribution of the GOCCP cloud fraction, together with the fractional area of each grid box (or each latitude) associated with clear-sky or undefined

situations, are shown in Figure 4. At each altitude, the sum of cloudy, clear, undefined areas is equal to 1. The zonal mean cloud fraction is maximal within the atmospheric boundary layer (below 3 km), except at very low latitudes where upper-level clouds mask lower-level clouds (as indicated by the maximum of the fully attenuated fraction). The mid-latitude cloudiness occurs at all levels of the atmosphere, with a maximum at low levels. Such a structure is expected in regions where baroclinic instabilities produce frontal clouds over the whole depth of the troposphere and where anticyclonic situations produce boundary-layer clouds. Equatorward of about 10° of latitude, the cloud fraction is greatest at heights between 12 and 14 km In the Tropics, this atmospheric layer corresponds to the layer where extensive anvil clouds are formed by the detrainment of hydrometeors from convective systems [e.g. Folkins et al., 2000]. The features of Figure 4 agree roughly with Figure 8 of [Mace et al., 2009], but the absolute values, especially for high clouds, are lower, again because of the different detection thresholds of thin cirrus by CALIOP-NASA and CALIOP-GOCCP.

The uncertain situations (Figure 4d) correspond to cases in which the SR signal is too high for a clear-sky situation, but is too low to unambiguously define the presence of a cloud layer. These situations may occur where boundary-layer aerosols are abundant (e.g. over the Atlantic windward of the Sahara), or where the cloudiness is too thin or too broken to pass the cloud detection threshold (SR=5).

(iii) SR histograms

Histograms of SR provide a summary of the occurrence of the different SR values encountered within a gridbox at a given altitude. Each histogram is normalized by dividing the occurrence in each SR-altitude box by the total number of occurrences in the histogram. This diagnostic is the lidar counterpart of the joint height-reflectivity histogram derived from Cloudsat radar data for comparable vertical grids [e.g. Zhang et al., 2007, Bodas et al., 2008, Marchand et al., 2009].

Figure 5 shows histograms of SR aggregated for various regions and for two seasons (JFM and JJA). Those exhibit different patterns depending on the prominent cloud types in presence. Over the Tropical Western Pacific warm pool, deep convective cloud systems produce many large SR values (> 10) at altitudes between 12 and 15 km (Fig. 5a) and numerous cases of fully attenuated values (SR < 0.01) below 8 km (related to the attenuation of the low-altitude lidar signal by the overlapping thick cloud layers). Secondary maxima in the SR histogram also appear in the mid-troposphere (5 - 9 km), which is consistent with the large abundance of thick congestus clouds over this region [Johnson et al., 1999], and at low-levels (below 3 km) associated with the presence of small shallow cumulus clouds. On the contrary, the SR histogram associated with California stratocumulus clouds exhibits two distinctive maxima: the first one below 3 km, where numerous low-level clouds produce a wide range of SR values between 3 and 80, and the second one around 10 km associated with the presence of thin cirrus clouds. Note that values of $3 < SR < 5$ above 14 km are due to observational noise and thus have no geophysical meaning; they do not pass the test, ATB-$ATB_{mol} < 2.5.10^{-3}$ km^{-1}.sr^{-1} (defined in Sect. 2b). In the mid-latitude North Pacific region, the SR histogram exhibits a large range of SR values over the whole troposphere and a substantial number of fully attenuated values below 5 km, consistent with the presence of thick, high-topped frontal clouds of large vertical extent in regimes of synoptic ascent (e.g. baroclinic fronts) and the presence of low-level clouds in regimes of synoptic descent [e.g., Lau and Crane, 1995; Norris and Iacobellis, 2005].

3. Sensitivity to horizontal sampling, vertical averaging, and to cloud detection thresholds.

(i)   Sensitivity to horizontal sampling

All the GOCCP cloud diagnostics are derived at the full horizontal resolution of CALIOP Level 1 data (330 m along the track below 8 km and 1 km above 8 km). They are based on

a procedure that, at this resolution, declares each atmospheric layer as totally "clear", "undefined", "fully attenuated" or "cloudy" (to be consistent with the lidar simulator). Because, as in nature, clouds exhibit a very wide range of sizes the cloud detection is sensitive to the horizontal resolution of the data. As a test of this sensitivity, we examined the impact of resolution on the diagnosed cloud fraction by horizontally averaging the lidar signal over each10 km prior to cloud detection. The results (not shown) indicate that the horizontal averaging can induce an artificial overestimate of the observed cloud cover in broken low cloud cumulus fields. The overestimate ranges up to about 20 to 25% in the trade cumulus regime. This can be understood by considering the following idealized example: a single low-level liquid water cloud of small size (e.g., 1-km radius) surrounded by clear-sky can produce locally a strong lidar backscattered signal (and thus a high SR value) which, once averaged with the surrounding clear sky profiles, can lead to an SR value passing the cloud detection threshold (SR=5). In such a case, a pixel of 10-km in length may thus be declared as overcast although the actual cloudiness covers only one hundredth of the area of that pixel.

The GOCCP cloud detection is thus made at the full resolution of the original CALIOP level 1 data to ensure that the cloud cover is not artificially overestimated in regions where clouds have typical sizes larger than or of the order of this resolution (75 m cross-track and 330 m along track below 8 km).

(ii) Sensitivity to the vertical grid resolution

A pre-requisite for a consistent model-data comparison of the cloud fraction is that cloud layers are defined similarly in observations and in model outputs. Using lidar signals to diagnose cloud layers requires that similar SR thresholds are used for cloud detection and that these thresholds are applied at the same vertical resolution. COSP diagnostics from climate models may be analyzed either at the vertical resolution of each model (which

varies from one model to another), or over a pre-defined vertical grid of 40 equidistant levels (the so-called "COSP grid"). Here, we examine the impact of vertical resolution on GOCCP cloud diagnostics.

The initial CALIOP L1 data contain 583 levels with 30-m spacing between the surface and 8 km and 60-m spacing above 8 km. As shown in Figure 1, averaging CALIOP L1 data over the 40-level grid significantly increases the signal-to-noise ratio, and therefore minimizes the risk of false cloud detections. Chepfer et al. [2008] derived the CALIPSO cloud fraction for a coarser vertical grid, corresponding to the 19 vertical levels of the standard version of the LMDZ4 GCM, with 6 levels at low altitudes (below 3 km), 3 levels at middle heights (between 3 and 7.2 km), and 10 levels in the upper troposphere (above 7.2 km). In the 40-level grid, the "low-level", "mid-level" and "upper-level" atmospheric layers are comprised of 7, 8 and 25 levels, respectively.

The total cloud cover obtained for 19 levels is about 0.05 lower than that for 40 levels (Table 1 and 2), but this discrepancy is much more significant for the upper-level cloud fraction (up to 0.20 difference over tropical continents in the Southern Hemisphere). Likewise, we examined the effect of increasing the GOCCP dataset to 80 levels at night (when signal to noise remains good at this vertical resolution) and found an increase in the cloud fraction of about 0.05. Vertical averaging lessens the contribution of optically thin cirrus clouds to the SR signal and, therefore, decreases the probability of passing the cloud detection threshold (Figure 1d). Thus, reducing the vertical resolution decreases the high-level cloud amount and, more generally, the cloud fraction associated with thin stratiform cloud layers. Figure 6 shows that this effect also impacts low and mid level cloud amounts with larger differences (up to 0.05) at latitudes poleward of 60°.

(iii) Sensitivity to the cloud detection threshold

The cloudy threshold value (here SR=5) is a parameter of the lidar simulator that affects the detection of the optically thinner clouds. The higher the SR threshold is, the lower the cloud fraction will be and the more optically thin clouds will be missed. Typically, assuming a homogeneous boundary layer water cloud with a geometrical thickness of 250 to 500 m and a liquid particle radius of 12 μm, a value SR=5 corresponds to an optical depth of 0.03 - 0.05 and an LWP of 0.1 - 0.2 g/m^2. Keeping all the others parameters constant, the optical depth will increase with the LWP and decrease when the particle size increases. Based on this estimate, most semi-transparent clouds (optical depth > 0.03) are detected, but most subvisible ones are missed. On the other hand, some very dense dust layer can be classified as cloudy when applying a simple cloud detection threshold based on SR alone. To test the sensitivity of our results to this threshold value, we computed cloud fractions for a threshold value of 3, which would detect clouds having an optical depth larger than about 0.015.

When the cloud detection threshold is reduced, the mean total cloud fractions increase by about 0.05 during night time and by up to 0.10 during daytime (Table 3). Figure 7 shows that the total cloud cover is shifted to greater values at all latitudes except over polar regions. High-level clouds (not shown) do not contribute significantly to this increase. Sub-visible clouds, that may occur, for instance, above the overshoot regions [Dessler, 2005], are missed by both thresholds (SR=3 and SR=5). The total cloud cover increase is primarily driven by the global increase of the tropical low-level cloud fraction (Table 3 and Fig. 7c). This latter results from a more frequent detection of optically thin and/or broken boundary layer clouds, most likely to be shallow cumulus. The mid-level cloud fraction also increases in the Tropics in the area of large deserts (Figure 7b) when decreasing the cloud detection threshold, especially for daily observations (Table 3). It may be that the SR=3 threshold detects some large smoke or dust loading events occurring in summer, and/or to the presence of thin clouds at the top of the Saharan atmospheric boundary layer.

4. Day-night and regional cloud variations.

(i) Day-night differences

The clear-sky daytime CALIOP data are much noisier than those at night (Figure 1 vs. Figure 2) because of the solar photons. About 30% of the daytime profiles are rejected after quality test on the normalization of CALIOP Level 1 V2 data (Sect. 2a). We examine the day-night cloud cover differences to check whether the daytime data introduce a bias in the mean day/night results. The total day-night cloud cover difference is small at the global scale (< 0.01, Table 1). The largest differences occur over continents where clouds are slightly more frequent during daytime at all altitudes (Table 1), but the day-night variation depends on the vertical resolution (Table 2 for the coarse grid vs. Table 1 for CFMIP) and on the cloudy threshold value (SR=3 or SR=5, Table 3).

Maps of day-night differences (Figure 8a) show that clouds are more frequent over continents during daytime (13:30 local time), whereas low-level clouds are more frequent (15%) during night-time (1:30 local time) than during daytime in the tropical subsidence regions. Examination of the low, mid, high cloud amounts independently reveals that the total day-night cloud cover variation is mostly driven by low level clouds (Figure 8b). Both the geographical patterns and the order of magnitude of the day-night differences are in agreement with the High Resolution Infrared Sounder (HIRS) observations reported by Wylie [2008]. Even though, it can not be fully asserted that the day-night variation found in GOCCP is not biased by the noise associated with solar photons (which is larger in area with bright clouds), while any bias effect is likely sufficiently small for GCM evaluation studies

(ii) A regional scale example: along the GPCI transect

14

To evaluate the cloudiness simulated by weather and climate models, the GEWEX Cloud System Study has defined a transect, named the GEWEX Pacific Cross-section Intercomparison (GPCI, http://www.igidl.ul.pt/cgul/projects/gpci.htm) transect (black line on Figure 3a), that samples the stratocumulus region off the coast of California (35°N), the trade winds associated with shallow cumulus clouds, and the deep convective regions of the ITCZ (0-12°N). The mean JJA cloud fractions along this transect are shown in Figure 9a. The stratocumulus and shallow cumulus remain below altitudes of 2400 m with most below 2000 m, and their top heights increase from 1 to 2 km away from the coast. Deep convective clouds are mostly located below 17 km, and the lidar signal is fully attenuated below 8 km (not shown), meaning that the mean cloud optical depth between 8 and 17 km is typically on the order of 3. (The optical depth of the total column can be much larger than that.) The low-level cloud fraction exceeds 0.70 (Figure 9b) along the coast and decreases southward where the mid and high cloud cover increases, masking some of the low clouds. The diagram of SR along the transect (not shown) exhibits two maxima at low altitudes: high values of SR (> 60) associated with stratocumulus clouds and low values (SR<20) corresponding to cumulus clouds.

5. Comparison with other cloud climatologies

The availability of satellite measurements for more than 25 years has led to several global climatologies of cloud properties. They are being intercompared within the framework of the GEWEX cloud assessment (http://climserv.ipsl.polytechnique.fr/gewexca, Stubenrauch et al., 2009).

(i) Description of other cloud climatologies

- ISSCP: The International Satellite Cloud Climatology Project (ISCCP, Rossow and Schiffer [1999]) has been deriving cloud properties since 1983 using data taken by geostationary and polar orbiting weather satellites. Average ISCCP cloud amounts were computed for the period from 1984 to 2004, using 3-hourly daytime measurements from one infrared (IR) and one visible (VIS) atmospheric window channel at a spatial resolution of about 7 km, sampled every 30 km. Clouds are detected through a variable IR-VIS threshold test which compares the measured radiances to 'clear sky composite' radiances that have been inferred from a series of statistical tests on the space and time variations of the IR and VIS radiances [Rossow et al., 1993]. These clear sky conditions are associated with low IR and VIS spatial and temporal variability.

- TOVS Path-B and AIRS-LMD: Due to their relatively good spectral resolution, IR sounders, like the HIRS of the TIROS-N Operational Vertical Sounder (TOVS) system aboard the National Oceanic and Atmospheric Administration (NOAA) satellites or the Atmospheric InfraRed Sounder (AIRS) aboard the Earth Observing Satellite (EOS) satellite Aqua, provide reliable cirrus detection, day and night. These data have been analyzed by Stubenrauch et al. [2006, 2008] to produce alternate long-term cloud climatologies, so far from 1987 to 1995 and from 2003 to 2008, respectively. Cloud properties have been determined at spatial resolutions of 100 km and 13 km, respectively. Whereas the TOVS Path-B cloud detection (at spatial resolution of about 17 km at nadir) is based on a combination of HIRS and Microwave Sounding Unit (MSU) measurements, the AIRS-LMD cloud retrieval, based on a weighted χ^2 method providing cloud pressure and cloud emissivity (Stubenrauch et al., 1999a; as TOVS Path-B), uses an 'a posteriori' identification of cloudy scenes: The χ^2 method is applied to all scenes, and in a second step non-physical results are rejected as clear or partly cloudy scenes [Stubenrauch et al., 2008].

- MODIS-CERES: A shorter term climatology of clouds is being derived from low-Earth orbiting satellites by the Clouds and the earth's Radiant Energy System (CERES) project,

which began in 1998 with the Tropical Rainfall Measuring Mission satellite, is currently operating aboard the EOS Aqua and Terra satellites, and will continue on other satellites in the future. The Aqua CERES cloud amounts and heights reported here were determined from MODerate-resolution Imaging Spectroradiometer (MODIS) data for the period July 2002-July 2007 using the methods of Minnis et al. [2008, 2009] and Trepte et al. [2002]. The results are denoted as CERES-MODIS data.

- PARASOL-PO2: The PARASOL cloud products for the period January 2006 – December 2008 are derived during daytime from multispectral (visible and near infrared only) and multiangle measurements from the Polarisation and Directionality of the Earth Reflectances (POLDER) instrument at a native resolution of 6 km x 6 km [Parol et al., 2004].

(ii) Comparison of CALIPSO-GOCCP with other cloud climatologies

Figure 10 presents the annually-averaged global cloud cover, separately for ocean and land areas, as obtained from CALIPSO GOCCP, ISCCP, AIRS-LMD, TOVS Path-B, CERES-MODIS and POLDER3/PARASOL. For a more consistent comparison between these cloud climatologies derived from passive remote sensing and GOCCP, a version of CALIPSO GOCCP (referred to as CALIPSO-GOCCP-5-no-overlap) has been treated in such a way that only the highest non-overlaped cloud layer is taken into account. All averages are area weighted. The total cloud cover varies from 58% to 76%, depending on the sensitivity of the instrument or the retrieval algorithm or the handling of partly cloudy footprints. All climatologies show ~10 percent more cloud cover over ocean than over land, with more lowlevel clouds over ocean than over land and about the same amount of high clouds over ocean and land. The cloud cover of AIRS-LMD is slightly less than that from TOVS Path-B and similar to that from ISCCP, because it corresponds to clouds for which cloud properties can be reliably determined (see above). When adding the eliminated partly cloudy footprints,

weighted by a factor of 0.3, the cloud fraction rises from 0.67 to 0.75, indicating the uncertainty of cloud cover due to partly cloudy footprints. CALIOP appears to be the instrument most sensitive to cirrus, providing a high cloud cover of about 32% for CALIOP-GOCCP-5 and 40% for CALIOP-NASA (Winker et al. 2008), while the IR sounders provide about 30%, ISCCP about 22.5%, MODIS-CERES 20% and PARASOL only about 10%. POLDER high cloud amount is much less than that of all other climatologies due to (i) its limited ability to detect thin high clouds (no IR channels available), (ii) because O_2 cloud apparent pressure is only derived over land for optical thicknesses greater than 2.0 and (iii) because O_2-derived cloud apparent pressure tends to correspond to the middle of cloud pressure level [Vanbauce et al., 2003]. Cirrus above low clouds are often misidentified as mid-level clouds by ISCCP [e.g. Stubenrauch et al., 1999b] as well as by POLDER and CERES-MODIS. This may explain why the mid-level cloud fraction from ISCCP is larger than that of other climatologies obtained from passive remote sensing and that obtained from Calipso when identifying only the uppermost cloud layer (CALIPSO-GOCCP-5-no-overlap).

The mid-level and low-level cloud fractions from CALIPSO-GOCCP-5 are larger than that derived from ISCCP, because in addition to the uppermost cloud layers, clouds which are overlapped by higher clouds are also taken into account. The comparison of CALIPSO-GOCCP-5 with CALIPSO-GOCCP-5-no-overlap shows that at a spatial resolution of 2.5° x 3.75° only about half of all low and mid-level clouds are single layer clouds. As a consequence, low-level cloud fractions determined by AIRS-LMD, CERES-MODIS, ISCCP and TOVS Path-B fall between CALIPSO-GOCCP-SR5 and CALIPSO-GOCCP-SR5-no-overlap (Figure 10). Reducing the spatial resolution will lead to a reduction of multi-layer clouds: Mace et al. [2009] have found that 24% of all cloud systems are multilayered at a spatial resolution of 1° x 1° (requiring a 1 km gap between different cloud layers).

6. Conclusion

A GCM-Oriented CALIPSO Cloud Product (GOCCP) has been developed from the CALIOP L1 dataset to make consistent comparisons between CALIOP observations and "GCM+lidar simulator" outputs. For this purpose, the full-horizontal-resolution CALIOP level 1 data were vertically averaged at a resolution comparable to that of GCMs (40 levels), and then simple thresholds were applied to SR profiles to classify each atmospheric layer as cloudy, clear, fully attenuated or unclassified. Maps of the total cloud fraction and of the low-mid-high layered cloud fractions, 3D vertical distributions of the cloud fraction and joint height-SR histograms were then analyzed. The sensitivities of the results to the vertical grid and to the value of the SR threshold used for cloud detection were also studied. When decreasing the cloudy SR threshold value, the cloud fraction increases because the optically thinnest layers are better detected, independent of altitude and surface type. The effect of changing the vertical resolution (from 40 equidistant levels to 19 sigma equidistant ones) is critical for all cloud categories.

The total and zonal mean cloud covers have been presented for two different seasons, JFM (January-February-March) and JJA (June-July-August) in accumulating 3 years of CALIOP observations (June 2006 to August 2008). The results show that large cloud fractions (> 40%) are located in the marine boundary layer and that they have a significant seasonal variability; the contribution of the Southern hemisphere tropical oceans is very significant. The seasonal variation of the global cloud cover is weak (less than 0.01), as is the globally-averaged day-night variation. On average, the cloud cover is greater over ocean than over land. Despite the enhanced noise of the lidar profiles in clear sky during daytime (resulting in the rejection of about 30% of the daytime profiles in this study), the day-night cloud cover difference seems robust and shows similar patterns and amplitude as the ones reported in the literature: more low-level clouds during night time in the oceanic subsidence regions and more clouds during

daytime over land. Marine low-level clouds exhibit two categories, associated with different ranges of SR values: optically thick clouds (SR > 60) and optically thin clouds (SR < 20) that can be attributed to different horizontal cloud structure or different microphysics (particle sizes). Selected regions (tropical Western Pacific, mid-latitude North Pacific, and California stratocumulus) exhibit different types of SR histograms, showing the potential of such diagrams for characterizing the prominent cloud types encountered in these regions.

As recommended by the WCRP Working Group for Coupled Models (http://eprints.soton.ac.uk/65383), the COSP simulator (version v1.0) developed by CFMIP (to be made available on http://www.cfmip.net) is to be used by the climate modeling groups in some of the CMIP5 simulations [Taylor et al., 2009] that will be assessed by the Fifth Assessment Report (AR5) of the Intergovernmental Panel on Climate Change (IPCC). The CALIPSO-GOCCP products presented in this paper are fully consistent with the outputs from the lidar simulator used in COSP v1.0, and they are available on-line through the GOCCP website (http://climserv.polytechnique.fr/cfmip-atrain) at two different horizontal resolutions: 1° x 1° and 2.5° x 2.5°. In the future, these data may thus be directly compared with the lidar simulator outputs from the CMIP5 simulations, and then be used to evaluate the cloudiness predicted by the different GCMs participating in CMIP5.

References

Bodas-Salcedo A., M. J. Web, M. E. Brook, M. A. Ringer, S. F. Milton, and D. R. Wilson, (2008), Evaluation of cloud systems in the Met Office global forecast model using CloudSat data, J. Geophys. Res., 113, D00A13, doi:10.1029/2007JD009620.

Bony S. and J-L. Dufresne (2005), Marine boundary layer clouds at the heart of tropical cloud feedback uncertainties in climate models, Geophys. Res. Lett., 32, No. 20, L20806, doi:10.1029/2005GL023851.

Bey, I., D. J. Jacob, R. M. Yantosca, J. A. Logan, B. D. Field, A. M. Fiore, Q. Li, H. Y. Liu, L. J. Mickley, M. G. Schultz (2001), Global modeling of tropospheric chemistry with assimilated meteorology: Model description and evaluation, J. Geophys. Res., 106(D19), 23073-23096, 10.1029/2001JD000807.

Chepfer, H., S. Bony, D. M. Winker, M. Chiriaco, J.-L. Dufresne, and G. Seze (2008), Use of CALIPSO lidar observations to evaluate the cloudiness simulated by a climate model, Geophys. Res. Lett., 35, L15704, doi:10.1029/2008GL034207.

Dessler A. E., S. P. Palm, W. D. Hart, J. D. Spinhirne (2006), Tropopause-level thin cirrus coverage revealed by ICESat/Geoscience Laser Altimeter System, J. Geophys. Res., 111, D08203, doi:10.1029/2005JD006586.

Dessler A. E., S. P. Palm, J. D. Spinhirne (2006), Tropical cloud-top height distributions revealed by the Ice, Cloud, and Land Elevation Satellite (ICESat)/Geoscience Laser Altimeter System (GLAS), J. Geophys. Res., 111, D12215, doi:10.1029/2005JD006705.

Folkins, I., S. Oltmans, and A. Thompson (2000), Tropical Convective Outflow and Near Surface Equivalent Potential Temperatures, Geophys. Res. Lett., 27(16), 2549-2552.

Haynes, J. M., R. T. Marchand, Z. Luo, A. Bodas-Salcedo, and G. L. Stephens (2007), A multipurpose radar simulation package: QuickBeam, Bull. Am. Meteorol. Soc., 88(11), 1723–1727, doi:10.1175/BAMS-88-11-1723

Johnson, R. H, T. M. Rickenback, S. A. Rutledge, P. E. Ciesielski, and W. H. Schubert (1999), Trimodal characteristics of tropical convection. J. Climate, 12, 2397-2418.

Klein S. A. and C. Jakob (1999), Validation and sensitivities of frontal clouds simulated by the ECMWF model. Mon. Wea. Rev., 127, 2514-2531.

Lau, N. C and M. W. Crane (1995), A satellite view of the synoptic-scale organization of cloud properties in midlatitude and tropical circulation systems. Mon. Wea. Rev., 123, 1984-2006.

Mace, G. G., Q. Zhang, M. Vaughan, R. Marchand, G. Stephens, C. Trepte, and D. Winker (2009), A description of hydrometeor layer occurrence statistics derived from the first year of merged Cloudsat and CALIPSO data. J. Geophys. Res., 114, D00A26, doi:10.1029/2007/JD009755.

Marchand, R., J. Haynes, G. G. Mace, T. Ackerman, and G. Stephens (2009), A comparison of simulated cloud radar output from the multiscale modeling framework global climate model with CloudSat cloud radar observations, J. Geophys. Res., 114, D00A20, doi:10.1029/2008JD009790.

Minnis, P., et al. (2008), Cloud detection in non-polar regions for CERES using TRMM VIRS and Terra and Aqua MODIS data, IEEE Trans. Geosci. Remote Sens., 46, 3857-3884.

Minnis, P., et al. (200p), Cloud property retrievals for CERES using TRMM VIRS and Terra and Aqua MODIS data, IEEE Trans. Geosci. Remote Sens., 46, 3857-3884.

Norris, J. R., and S. F. Iacobellis (2005), North Pacific cloud feedbacks inferred from synoptic-scale dynamic and thermodynamic relationships. J. Climate, 18, 4862-4878.

Parol F., J.C. Buriez, C. Vanbauce, J. Riedi, L. C.-Labonnote, M. Doutriaux-Boucher, M. Vesperini, G. Sèze, P. Couvert, M. Viollier, F.M. Bréon (2004), Capabilities of multi-angle polarization cloud measurements from satellite: POLDER results., Adv. Space Res. , 33, 1080-1088

Rossow, W. B. and R. A. Schiffer (1999), Advances in understanding clouds from ISCCP, Bull. Amer. Meteor. Soc., 80, 2261-2287.

Rossow, W. B. and L. C. Garder (1993), Cloud detection using satellite measurements of infrared and visible radiances for ISCCP. J. Climate, 6, 2341-2369.

Sassen, K. and Z. Wang (2008), Classifying clouds around the globe with the CloudSat radar: 1-year of results, Geophys. Res. Lett., 35, L04805, doi:10.1029/2007GL032591.Stubenrauch, C. J., A. D. Del Genio, and W. B. Rossow (1997), Implementation of Sub-Grid Cloud Vertical Structure inside a GCM and its Effect on the Radiation Budget, J. Climate, 10, 273-287

Stubenrauch, C. J., A. Chédin, R. Armante, and N. A. Scott (1999a), Clouds as seen by Infrared Sounders (3I) and Imagers (ISCCP): Part II) A New Approach for Cloud Parameter Determination in the 3I Algorithms, J. Climate, 12, 2214-2223.

Stubenrauch, C. J., W. B. Rossow, N. A. Scott, and A. Chédin (1999b), Clouds as seen by Infrared Sounders (3I) and Imagers (ISCCP): Part III) Spatial Heterogeneity and Radiative Effects. J. Climate, 12, 3419-3442.

Stubenrauch, C. J., A. Chédin, G. Rädel, N. A. Scott, and S. Serrar (2006), Cloud properties and their seasonal and diurnal variability from TOVS Path-B, J. Climate, 19, 5531-5553.

Stubenrauch C., S. Cros, N. Lamquin, R. Armante, A. Chedin, C. Crevoisier, and N. A. Scott (2008), Cloud properties from atmospheric infrared sounder and evaluation with cloud-aerosol lidar and infrared pathfinder satellite observations. J. Geophys. Res., 113, D00A10, doi:10.1029/2008JD009928.

Taylor, K. E., R. J. Stouffer, and G. A. Meehl (2009), A summary of the CMIP5 Experiment Design (http://www.clivar.org/organization/wgcm/references/Taylor_CMIP5_dec31.pdf).

Trepte, Q., P. Minnis, and R. F. Arduini (2002), Daytime and nighttime polar cloud and snow identification using MODIS data, Proc. SPIE 3rd Intl. Asia-Pacific Environ. Remote

Sensing Symp. 2002: Remote Sens. of Atmosphere, Ocean, Environment, and Space, Hangzhou, China, October 23-27, Vol. 4891, 449-459.

Vanbauce C., B. Cadet, R. T. Marchand (2003), Comparison of POLDER apparent and corrected oxygen pressure to ARM/MMCR cloud boundary pressures, Geophys. Res. Letters , 30-5, 16.1 – 16.4, doi:10.1029/2002GL016449

Webb M, C Senior, S Bony and J-J Morcrette (2001), Combining ERBE and ISCCP data to assess clouds in three climate models, Climate Dynamics, 17, 905-922.

Winker D., W. Hunt, and M. McGill (2007), Initial Performance Assessment of CALIOP, Geophys. Res. Lett., 34, L19803, doi:10.1029/2007GL030135.

Winker D., B. Getzewitch, and M. Vaughan (2008), Evaluation and applications of Cloud Climatologies from CALIOP, ILRC conf. REF?

Winker D., M. A. Vaughan, A. Omar, Y. Hu, K. A. Powell, Z. Liu, W. H. Hunt, and S. A. Young (2009), Overview of the CALIPSO mission and CALIOP data processing algorithms, J. Atmos. Ocean. Tech, in press

Wylie D. (2008), Diurnal cycles of clouds and how they affect polar-orbiting satellite data, J. Clim. 21, 3989-3996.

Zhang M H, W Y Lin, S A Klein, J T Bacmeister, S Bony, R T Cederwall, A D Del Genio, J J Hack, N G Loeb, U Lohmann, P Minnis, I Musat, R Pincus, P Stier, M J Suarez, M J Webb, J B Wu, S C Xie, M -S Yao and J H Zhang (2005), Comparing Clouds And Their Seasonal Variations in 10 Atmospheric General Circulation Models With Satellite Measurements. J. Geophys. Res., 110, D15S02, doi:10.1029/2004JD005021.

Table 1: Cloud fraction from standard GOCCP (detection threshold SR=5 and COSP vertical grid of 40 equidistant vertical levels) for two seasons (JFM=January-February-March and JJA=June-July-August).

GOCCP		JFM Night	JJA Night	JFM Day	JJA Day
Global	**Total**	**0.66**	**0.66**	**0.66**	0.66
	Low	0.36	0.36	0.36	0.37
	Mid	0.20	0.19	0.27	0.25
	High	0.29	0.29	0.35	0.33
Land	**Total**	**0.55**	**0.54**	**0.61**	0.61
	Low	0.20	0.15	0.26	0.25
	Mid	0.26	0.24	0.32	0.31
	High	0.28	0.31	0.34	0.34
Ocean	**Total**	**0.71**	**0.71**	**0.68**	0.68
	Low	0.44	0.45	0.41	0.42
	Mid	0.18	0.17	0.24	0.23
	High	0.29	0.28	0.35	0.33

Table 2: Sensitivity to the vertical grid – cloud fraction diagnosed as in GOCCP but using a coarse vertical grid (19 vertical levels) instead of 40 levels.

Coarse GRID		JFM Night	JJA Night	JFM Day	JJA Day
Global	**Total**	**0.62**	**0.62**	**0.59**	0.60
	Low	0.34	0.34	0.35	0.36
	Mid	0.21	0.21	0.19	0.19
	High	0.16	0.16	0.16	0.16
Land	**Total**	**0.48**	**0.46**	**0.47**	0.49
	Low	0.16	0.12	0.20	0.19
	Mid	0.24	0.25	0.22	0.23
	High	0.15	0.17	0.13	0.14

Ocean	Total	0.68	0.68	0.64	0.65
	Low	0.42	0.44	0.42	0.43
	Mid	0.20	0.19	0.17	0.17
	High	0.16	0.16	0.16	0.16

Table 3: Sensitivity to the detection threshold – Cloud fraction diagnosed as in GOCCP but using a threshold value SR=3 instead of SR=5 for cloud detection.

JJA / Night		GOCCP SR3	GOCCP SR5	GOCCP Coarse Grid SR3	GOCCP Coarse Grid SR5
Global	**Total**	**0.70**	**0.66**	**0.68**	**0.62**
	Low	0.41	0.36	0.41	0.34
	Mid	0.21	0.19	0.22	0.21
	High	0.29	0.29	0.16	0.16
Land	**Total**	**0.57**	**0.54**	**0.49**	**0.46**
	Low	0.18	0.15	0.14	0.12
	Mid	0.27	0.24	0.26	0.25
	High	0.31	0.31	0.17	0.17
Ocean	**Total**	**0.76**	**0.71**	**0.76**	**0.68**
	Low	0.51	0.45	0.53	0.44
	Mid	0.18	0.17	0.20	0.19
	High	0.28	0.28	0.16	0.16

JJA / Day		GOCCP SR3	GOCCP SR5	GOCCP Coarse Grid SR3	GOCCP Coarse Grid SR5
Global	**Total**	**0,74**	**0.66**	**0,68**	**0.60**
	Low	0,46	0.37	0,46	0.36
	Mid	0,33	0.25	0,21	0.19
	High	0,34	0.33	0,16	0.16
Land	**Total**	**0,69**	**0.61**	**0,53**	**0.49**
	Low	0,33	0.25	0,24	0.19
	Mid	0,40	0.31	0,26	0.23
	High	0,35	0.34	0,14	0.14
Ocean	**Total**	**0,76**	**0.68**	**0,76**	**0.65**
	Low	0,52	0.42	0,57	0.43
	Mid	0,30	0.23	0,18	0.17
	High	0,34	0.33	0,17	0.16

Figure 1: One Orbit.

(a) Attenuated Backscattered (ATB) signal, Caliop level 1product, 583 vertical levels
(b) Lidar Scattering Ratio (SR) over the 40 vertical equidistant levels grid
(c) GOCCP diagnostics: cloudy, clear, uncertain, fully attenuated (SAT), below the surface level (SE).
(d) Example of one single vertical profile of the scattering ratio for the standard 40 levels grid and the coarse 19 levels grid: vertical bars correspond to the diagnostic thresholds (SR=5, SR=1.2, SR=0.01). The red horizontal lines show the limits of the low-mid-high atmospheric layers.

Figure 2: Same as 1 for one day time orbit. In c), the white lines correspond to regions where the profiles have been rejected because the noise was too large (see text).

Figure 3: GOCCP (a, b) total (c, d) upper-level (e, f) middle-level and (g,h) low-level cloud fraction (averaged over day and night) for JFM (left column) and JJA (right column).

Figure 4: Vertical distributions of the GOCCP cloud fraction for JJA and JFM (GOCCP-SR5) Zonally-averaged fractions of the longitude-latitude gridboxes flagged as Cloudy ((a) for JJA, (b) for JFM),(c) Clear JJA, (d) Uncertain JJA.
In each longitude-latitude gridbox and each atmospheric layer, the sum of the fractions (a)+(c)+(d) = 1.
The red horizontal lines show the limits of the low-mid-high atmospheric layers used to defined the layered cloud fractions.

Figure 5: Joint height-SR histogram for JFM (left column) and JJA (right column) derived from GOCCP night-time data for four different regions, from the top to the bottom :
Tropical Western Pacific (5°S-20°N ; 70°-150°E)
California Stratus Region (15-35°N ; 110-140°W)
North Pacific (30-60°N ; 160°E-140°W)
On each plot, the vertical axis is the altitude (in km) and the horizontal axis is the SR value.

Figure 6: Sensitivity to the vertical grid day/night
Zonal mean (a, e) total (b, f) upper-level (c, g) middle-level and (d, h) low-level cloud fraction (averaged over day and night) for JFM and JJA. above land (black), above sea (blue), and global (red). The lines without symbols are for the 40 levels grid and the lines with crosses for the coarse grid.

Figure 7: Difference between the cloud fractions diagnosed with a cloud detection threshold SR=3 and SR=5 (JJA, day/night average)
a) Total b) Mid c) Low cloud fraction

Figure 8 : Cloud cover difference between Day-time and Night-time GOCCP data for JJA

Figure 9: Cloud Fraction along the GCSS Pacific Cross-Section Intercomparison (GPCI) transect (that extends over the Pacific from California to the ITCZ) in JJA
(a) Vertical distribution of the Cloud fraction (b) Low, Mid, High and total cloud fractions

Figure 10: Comparison of GOCCP with others climatologies (annual means).
O= Ocean, L= Land
CALIPSO-GOCCP-SR5 (06-08) , same with no overlap (no cloud above), CALIPSO-GOCCP-SR3 (06-08), AIRS-LMD (03-08) , ISCCP (84-04), MODIS-CERES (02-07), TOVS-B (87-95), PARASOL/POLDER (06-08)

(a) ATB CALIPSO 01/01/2007 NIGHT
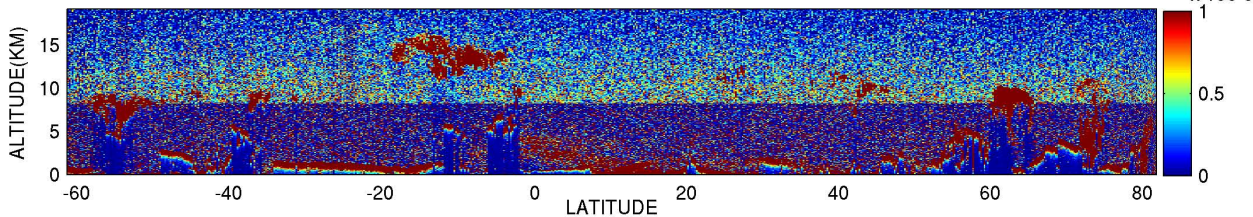
(b) SRMOY GOCCP 01/01/2007 NIGHT
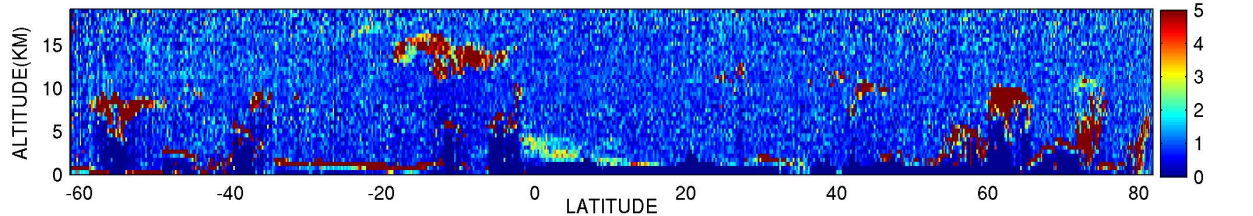
(c) DIAGNOSTICS GOCCP 01/01/2007 NIGHT
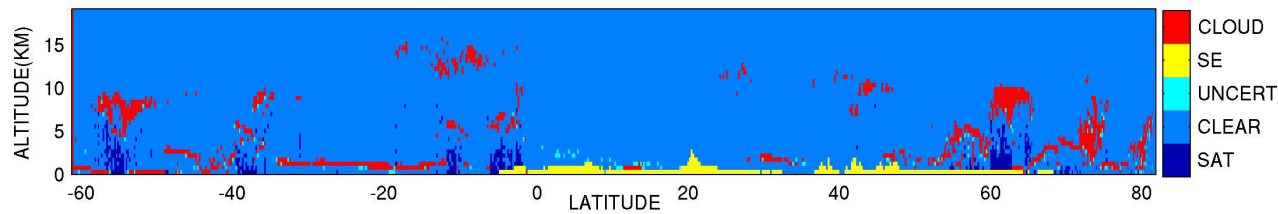
(d) GOCCP Grid vs COARSE Grid 01/01/2007 NIGHT
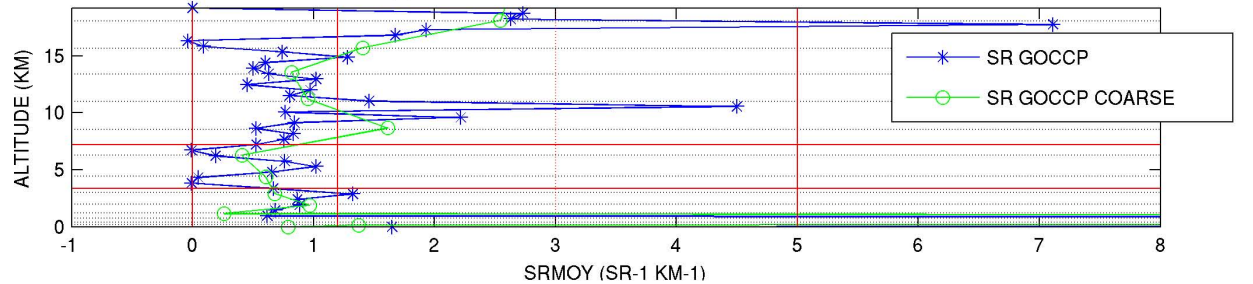
(a) ATB CALIPSO 01/01/2007 DAY
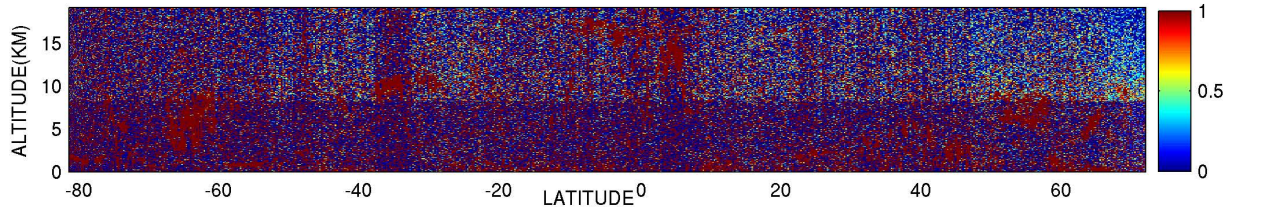
(b) SRMOY GOCCP 01/01/2007 DAY
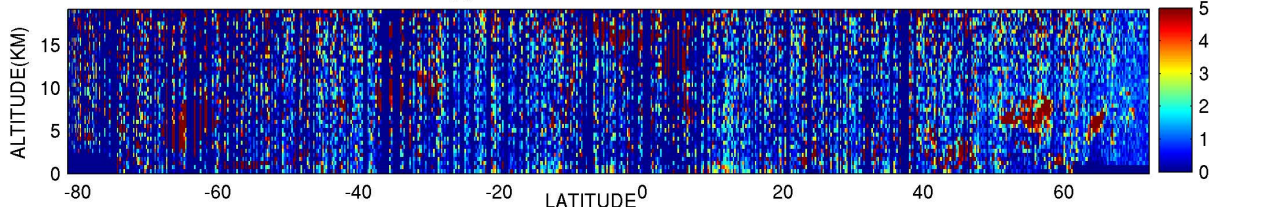
(c) DIAGNOSTICS GOCCP 01/01/2007 DAY
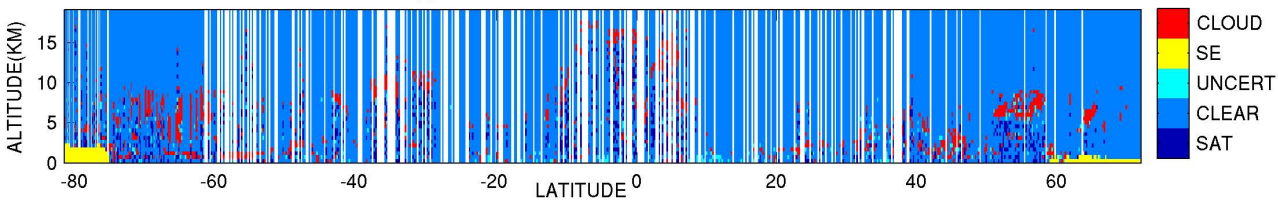
(d) SRMOY GOCCP Grid vs COARSE Grid 01/01/2007 DAY
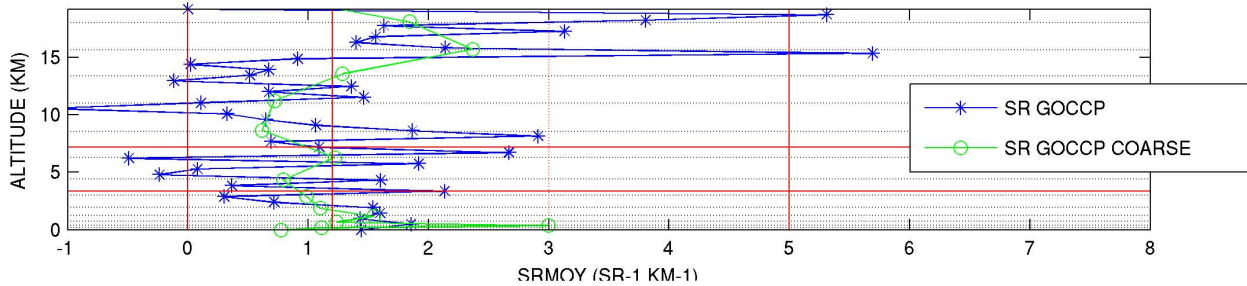
TOTAL CLOUD GOCCP JFM
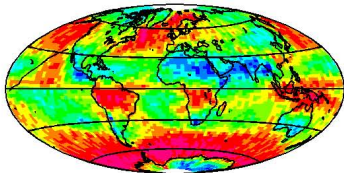
TOTAL CLOUD GOCCP JJA
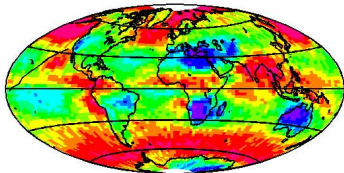
HIGH CLOUD GOCCP JFM
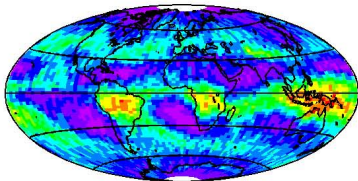
HIGH CLOUD GOCCP JJA
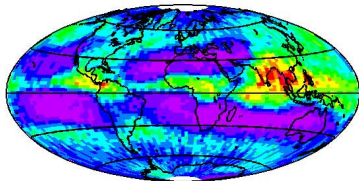
MID CLOUD GOCCP JFM
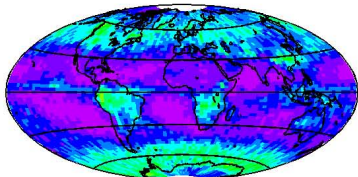
MID CLOUD GOCCP JJA
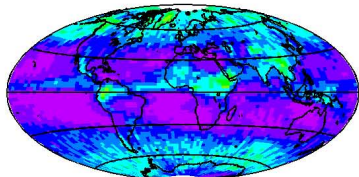
LOW CLOUD GOCCP JFM
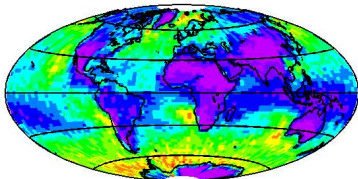
LOW CLOUD GOCCP JJA
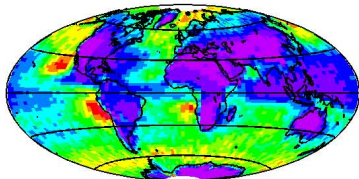
(a) CLOUD FRACTION JJA GOCCP
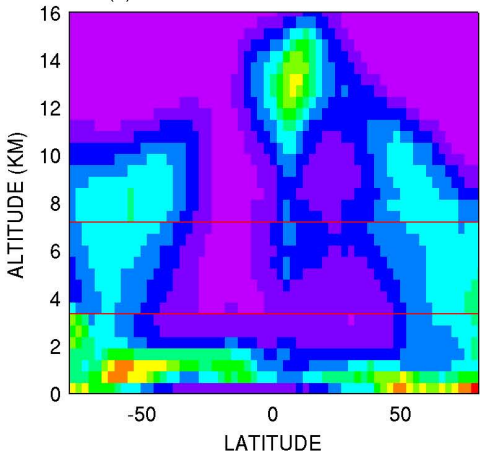
(b) CLOUD FRACTION JFM GOCCP
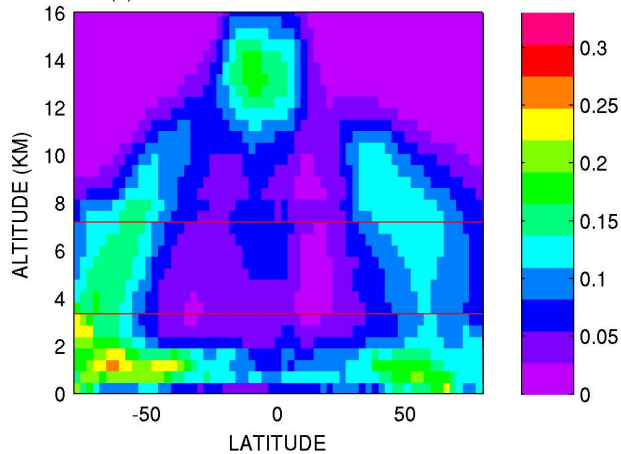
(c) CLEAR FRACTION JJA GOCCP
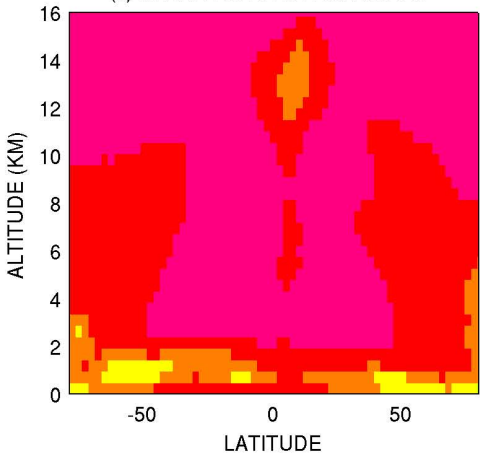
(d) UNCERT FRACTION JJA GOCCP
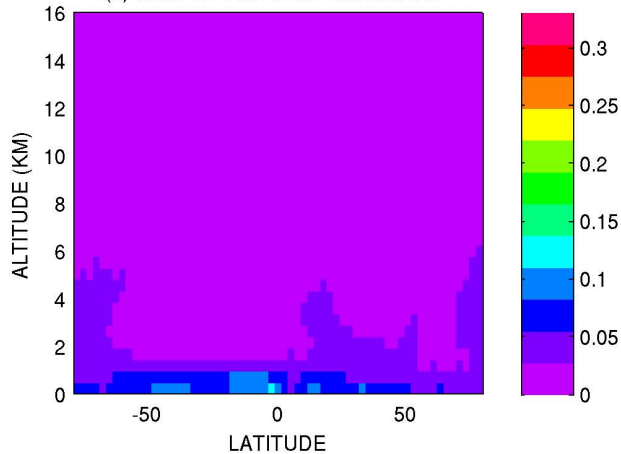
(a) SR histo Tropical Western Pacific JFM GOCCP
(d) SR histo Tropical Western Pacific JJA GOCCP
(b) SR histo California StratoCumulus JFM GOCCP
(e) SR histo California StratoCumulus JJA GOCCP
(c) SR histo Mid Latitude North Pacific JFM GOCCP
(f) SR histo Mid Latitude North Pacific JJA GOCCP
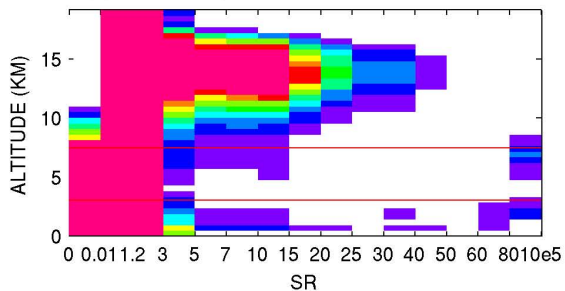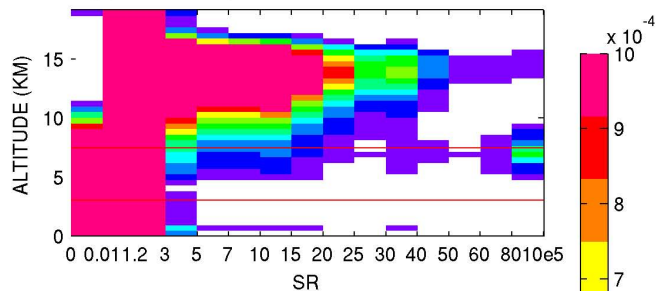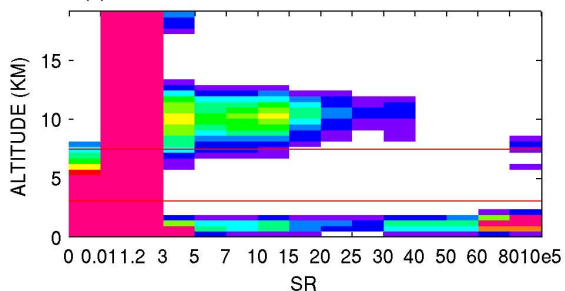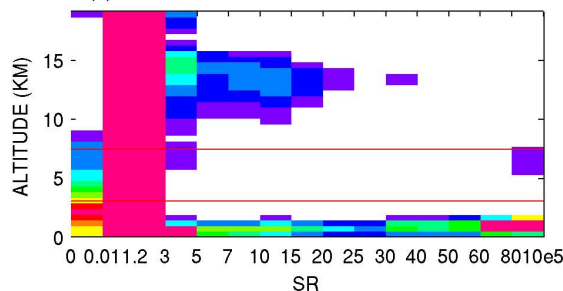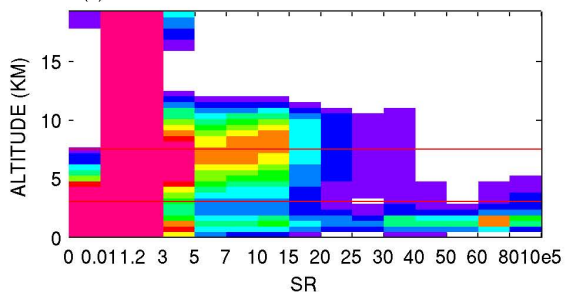
(a) TOTALCLOUD ZONAL MEAN JFM

(b) HIGHCLOUD ZONAL MEAN JFM

(c) MIDCLOUD ZONAL MEAN JFM

(d) LOWCLOUD ZONAL MEAN JFM

(e) TOTALCLOUD ZONAL MEAN JJA

(f) HIGHCLOUD ZONAL MEAN JJA

(g) MIDCLOUD ZONAL MEAN JJA

(h) LOWCLOUD ZONAL MEAN JJA

GOCCP land
GOCCP sea
GOCCP total
GOCCP COARSE land
GOCCP COARSE sea
GOCCP COARSE total
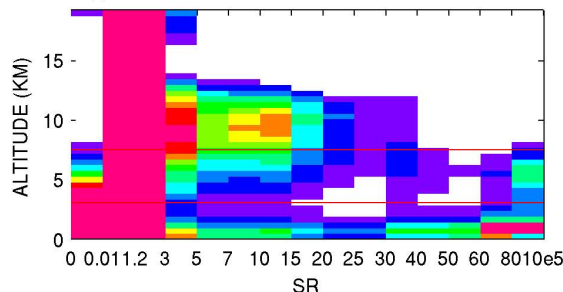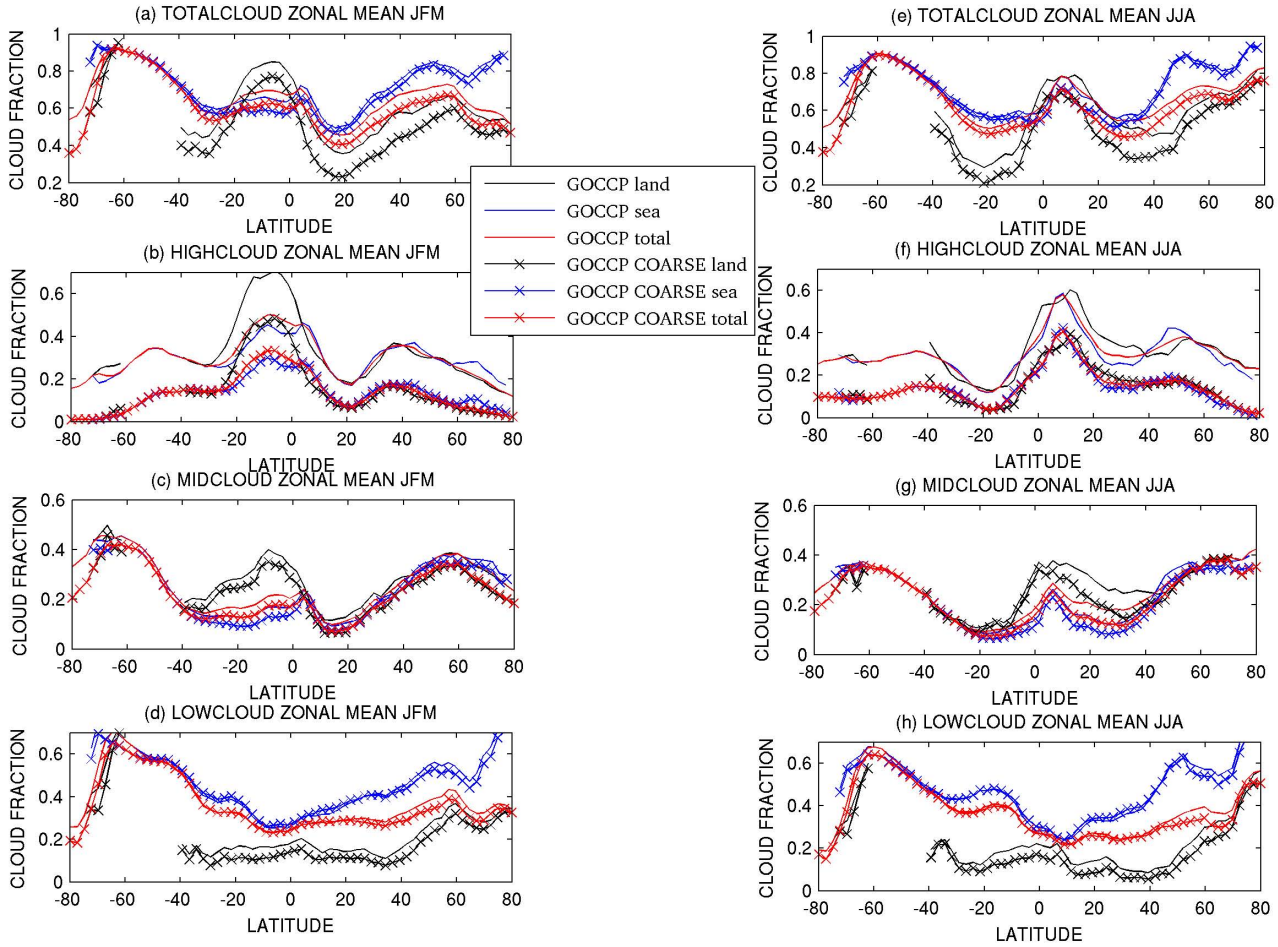
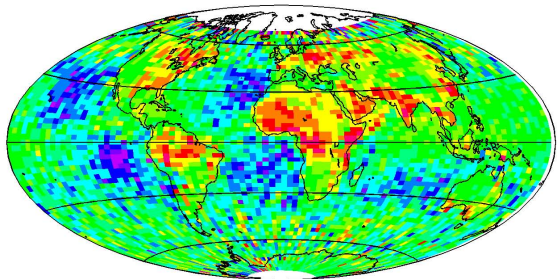(a) TOTAL CLOUD GOCCP JJA SR3-SR5
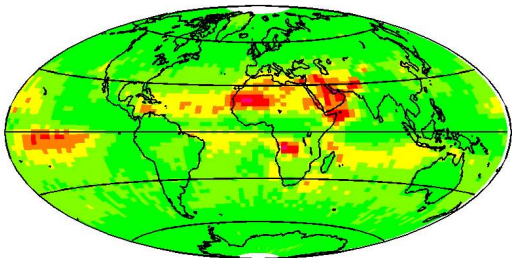
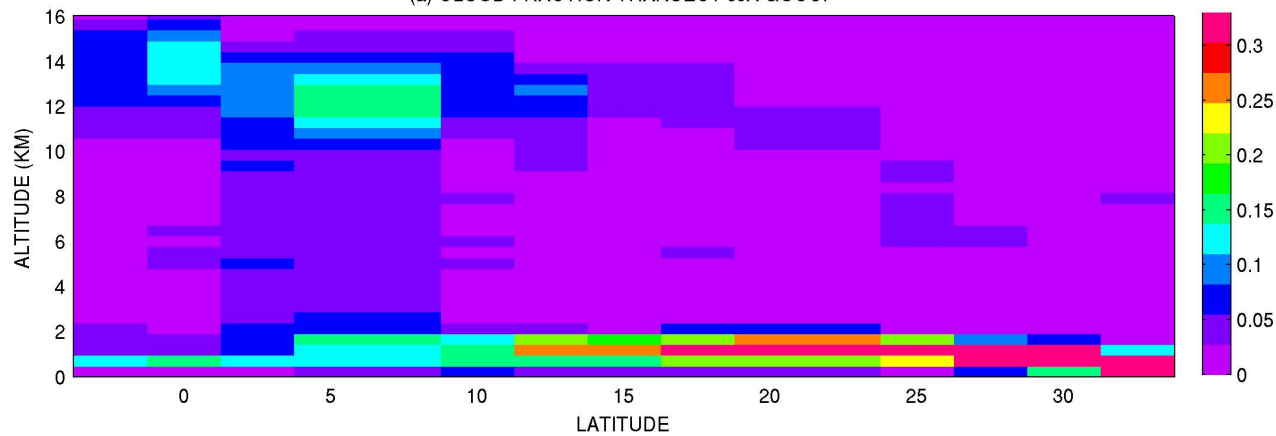(b) MID CLOUD GOCCP JJA SR3-SR5
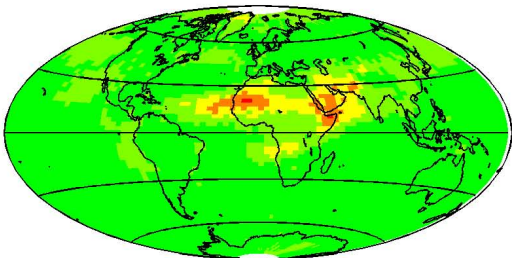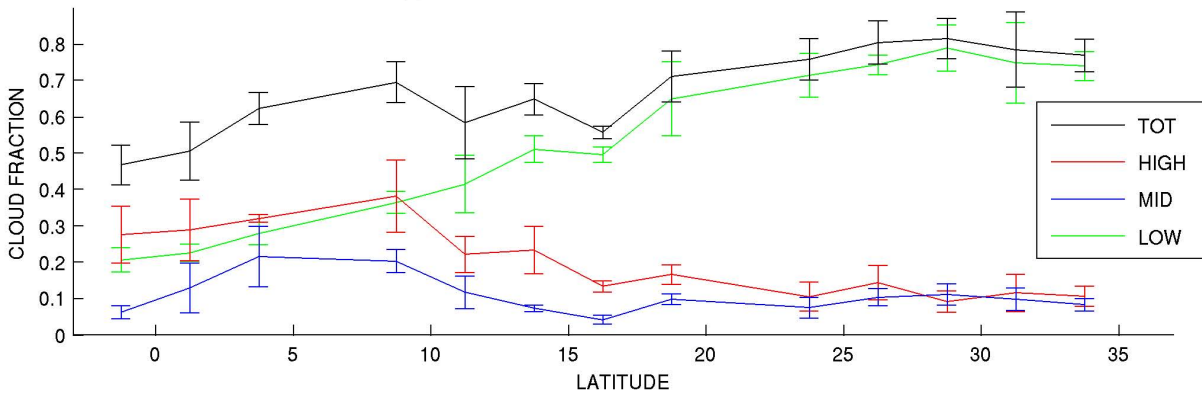
(c) LOW CLOUD GOCCP JJA SR3-SR5
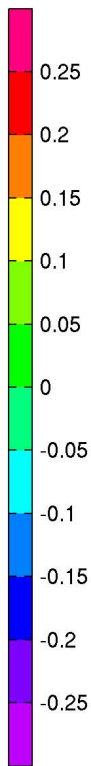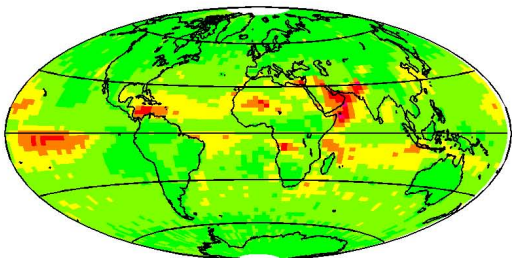
TOTAL CLOUD GOCCP JJA DAY-NIGHT
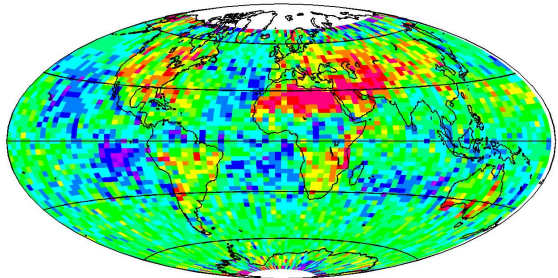
LOW CLOUD GOCCP JJA DAY-NIGHT
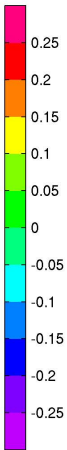
(a) CLOUD FRACTION TRANSECT JJA GOCCP

(b) ZONALMEAN TRANSECT JJA 2006 2007 2008